PCCP

RSC Publishing

PAPER

View Article Online
View Journal | View Issue

Cite this: *Phys. Chem. Chem. Phys.*, 2013, **15**, 489

Suppression of Sr surface segregation in $La_{1-x}Sr_xCo_{1-y}Fe_yO_{3-\delta}$: a first principles study

Hepeng Ding,[a] Anil V. Virkar,[a] Meilin Liu[b] and Feng Liu*[a]

Received 7th September 2012,
Accepted 1st November 2012

DOI: 10.1039/c2cp43148c

www.rsc.org/pccp

Based on systematic first principles calculations, we investigate Sr surface segregation (SSS) in $La_{1-x}Sr_xCo_{1-y}Fe_yO_{3-\delta}$ (LSCF) (a typical perovskite ABO_3 compound), a bottleneck causing efficiency degradation of solid oxide fuel cells. We identify two basic thermodynamic driving forces for SSS and suggest two possible ways to suppress SSS: applying compressive strain and reducing surface charge. We show that compressive strain can be applied through doping of larger elements and surface coating; surface charge can be reduced through doping of higher-valence elements in the Sr- and B-site or lower-valence elements in the La-site and introducing surface A-site vacancies. The net effect of oxygen vacancy is to enhance SSS because its effect of increasing surface charge overrides its effect of inducing compressive strain, while Co substitution of Fe always enhances SSS because it induces tensile strain as well as increases surface charge. Our results explain the recent experimental observation of SSS suppression in LSCF by a $La_{1-x}Sr_xMnO_{3-\delta}$ (LSM) coating.

1. Introduction

Solid oxide fuel cells (SOFCs) have the potential to be a clean and efficient power generation technology; however, the high operating temperature often poses material durability and engineering challenges.[1] To lower the cost of SOFC technology (*e.g.*, ~\$150 kW^{-1} by 2015[2]) and improve cell stability, it is necessary to reduce the operating temperature and use mixed electronic and ionic conductors as cathodes. In particular, $La_{1-x}Sr_xCo_{1-y}Fe_yO_{3-\delta}$ (LSCF) serves as a promising cathode material for intermediate-temperature SOFCs[3] because of its high electronic and ionic conductivity. However, the LSCF-based cathodes face severe efficiency degradation over time, typically at a rate of 0.05% $hour^{-1}$.[4] To date, a number of possible degradation mechanisms have been proposed, including interaction between LSCF and yttria-stabilized zirconia (YSZ),[5] Cr contamination,[6] coarsening of the cathode microstructure,[7] loss of conductivity,[8] and the widely believed Sr surface segregation (SSS) in LSCF cathodes.[9] The enrichment of Sr at the cathode surface may de-activate sites for oxygen reduction reaction and hence increase cathode resistance.[10–12]

It has been widely reported that SSS occurs in many $La_{1-x}Sr_xBO_3$ (B is Co, Fe, Mn, *etc.*) perovskite cathode materials, leading to various product phases on the surface or interface. Heide[13] reported a general Sr enrichment at all surfaces by a factor of ~1.2 to 2 times their stoichiometric values, forming SrO, then it may further react with CO_2 forming $SrCO_3$ at low temperatures. Elshof *et al.*[14] found that Sr segregates at both sides of the membrane, forming $SrCO_3$ and $SrSO_4$. Oh *et al.*[6] reported that the Sr segregation factor is approximately 2 and this is accompanied by the reduction in transition metal concentration at the surface, forming SrO and $SrCrO_4$. Mai *et al.*[5] found formation of insulating zirconate phases, such as $SrZrO_3$, at the LSCF cathode/YSZ electrolyte interface.

While SSS has been observed under various experimental conditions, the underlying mechanism is not completely clear, hindering the efforts to effectively suppress SSS. Several possible reasons have been proposed for SSS, such as kinetic demixing which is due to the greater mobility of Sr than other cations under oxygen partial pressure,[11,12] acid–base reaction where electropositive Sr works as a base while O_2 and Cr vapor species serve as acids,[6] different surface free energies and different atomic sizes,[15] and surface charge effect due mainly to electrostatic contributions.[16] But until now there is no established generally accepted theory yet. More recently, Lynch *et al.*[17] reported that upon $La_{1-x}Sr_xMnO_3$ (LSM) coating on LSCF, there is no obvious observation of SSS. The suppression of SSS in LSCF under LSM coating opens a possibility to increase the cathode durability, making mechanism investigation crucial to give guidance to future experiments. The Solid State Energy Conversion Alliance (SECA) requirement for SOFC efficiency degradation of less

[a] *Department of Materials Science and Engineering, University of Utah, Salt Lake City, Utah 84112, USA. E-mail: fliu@eng.utah.edu*
[b] *School of Materials Science and Engineering, Georgia Institute of Technology, 771 Ferst Dr, NW, Atlanta, GA 30332-0245, USA*

than 0.001% hour^{-1}, also calls for a better understanding of the suppression of SSS.

For a typical surface, it is widely recognized that surface stress plays an important role in determining surface properties[18,19] and a flat, strain free surface is naturally unstable under sinusoidal surface perturbations having a wave number greater than a critical value,[20] and strain relaxation can be partially accomplished by redistribution of ions with different sizes.[21] Also, it is well known that when there is an asymmetrically charged surface present in a crystal, the dipole moment perpendicular to the surface results in divergence of the long-range electrostatic interaction energy, making the surface unstable.[22] In principle, the polar surface can be stabilized by neutralizing the surface charge, such as *via* redistribution of ions with different charges. Hence, we expect that strain and surface charge will play an essential role in SSS in LSCF, because Sr and La have different charges and ionic radii.

To gain more insight to better understand the underlying mechanisms for SSS and in the hope of finding ways to suppress SSS (important for developing high efficiency SOFCs), we have employed a first principles density functional theory (DFT) computational method to systematically study SSS in LSCF. We first identified two basic thermodynamic driving forces for SSS, which are illustrated by studying the effect of strain and surface charge (through doping) on SSS. Then we suggest two common factors for suppressing SSS: applying compressive strain and reducing surface charge, and we verified our findings by studying the dependence of SSS on oxygen vacancy formation, Co substitution of Fe and cation deficiency. Moreover, we provide a possible explanation for the recently observed LSM-coating effect on SSS in LSCF.[17]

2. Computational method

The spin-polarized calculations are performed using VASP,[23] a plane wave based *ab initio* simulation package. The commonly used composition for LSCF is $La_{0.4}Sr_{0.6}Co_{0.2}Fe_{0.8}O_{3-\delta}$ in SOFCs due to its good thermo mechanical stability. But in order to reduce the system size, $La_{0.5}Sr_{0.5}Co_{0.25}Fe_{0.75}O_{3-\delta}$ was used in this study as a model system. Supercells of a 12-layer slab containing $2 \times 1 \times 6$ of the ABO_3 primitive unit cell and 20 Å vacuum are constructed to model the LSCF surface. For the $La_{0.5}Sr_{0.5}MnO_3$ (LSM) coating, a 4-layer LSM is added ($\sim$1.5% lattice mismatch). To improve the accuracy of the calculation, a $4 \times 8 \times 1$ *k*-point mesh and 800 eV kinetic energy cutoffs (the hard potential for O is chosen) are used, which leads to an energy convergence within 1 meV per atom when a force convergence criterion of 0.01 eV Å^{-1} was used. Perdew–Burke–Ernzerhof (PBE) exchange–correlation functional with the projector-augmented-wave approach is used except for the B-site transition metal elements which are treated by the PBE+U method with U_{eff} = 3.3, 4.0, and 4.0 eV for Co, Mn, and Fe, respectively.[24] Dipole correction ($\sim$0.9 electron Å) is added for all slab calculations. Charge analysis is done by the Bader charge analysis tool.[25] In studying the strain effect, in-plane lattice constants of the slab (normal to surface) are systematically changed for the given bi-axial strain values (Fig. 1(b) below) while the *z*-coordinates of all atoms are fully relaxed. This may correspond to the situation where the SSS predominantly occurs in surface regions with the underneath bulk remaining intact, so that effective surface layers are strained by the underlying bulk. To theoretically study the effect of strain due to oxygen vacancy, Co substitution of Fe, and doping of other elements, the in-plane lattice constants of the slab are fixed at the computational equilibrium LSF lattice constants with all the internal atomic coordinates optimized.

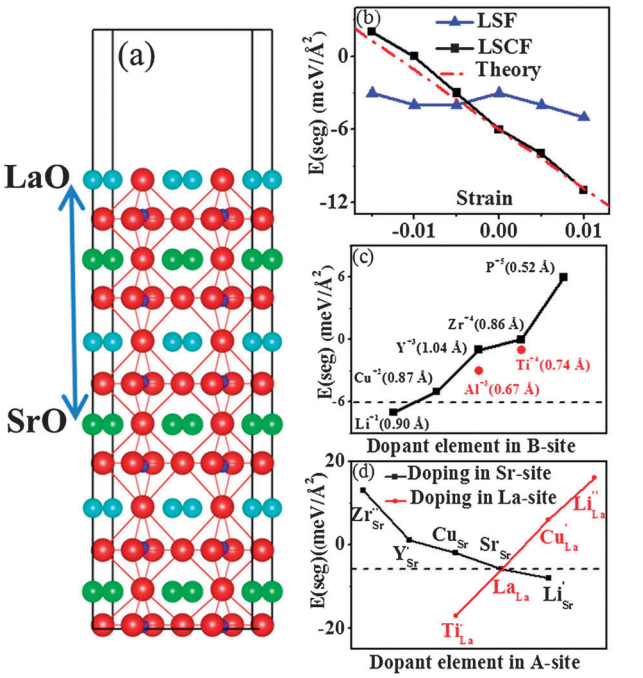

Fig. 1 (a) Illustration of SSS segregation with SrO exchanging with LaO indicated by the arrow. Cyan balls are La atoms, green are Sr, red are O, and small blue are Fe. (b) Effect of strain on SSS in LSF and LSCF. Squares are DFT+U calculated *E*(seg) and the dashed red line is the theory predicted dependence from eqn (5) using the DFT+U calculated surface segregation stress. (c) Effect of the B-site dopant on SSS. (d) Effect of the A-site dopant on SSS. The dotted horizontal line in (c) and (d) is *E*(seg) without doping.

As the first attempt, we focus our study on the SSS at the clean surfaces of a single phase of LSCF. In real SOFC operation, SSS actually occurs at the cathode/electrolyte (*e.g.*, LSCF/YSZ) interfaces, so that the presence of YSZ may play an important role in affecting the SSS. However, we believe the fundamental knowledge we learn from the simpler case of SSS in LSCF may still shed some lights on understanding the more complex process of SSS in the SOFC operation. We also note that another relevant phenomenon to the SSS is SrO phase separation. It is reported that LSCF reacts with YSZ forming $SrZrO_3$ (ref. 5) while it does not react with gadolinia doped ceria (GDC).[26] Consider the following two reactions:

$$SrO + ZrO_2 = SrZrO_3 \quad (1)$$

$$SrO + CeO_2 = SrCeO_3, \quad (2)$$

which describe the chemical reaction of LSCF in contact with YSZ and GDC, respectively. Assuming the activities of ZrO_2, CeO_2, $SrZrO_3$, and $SrCeO_3$ to be 1 and using Gibbs free energy data[27] derived at 1100 K, we obtain the activity of SrO to be 5.45×10^{-5} for reaction (1) and 4.61×10^{-3} for reaction (2), respectively. This suggests that the activity of SrO in LSCF is between 5.45×10^{-5} and 4.61×10^{-3}, indicating there is no obvious SrO phase separation for LSCF itself in the absence of YSZ or other oxide with which it reacts. We will leave the effect of YSZ on SSS and SrO phase separation for future studies. We also note that all of our calculations are performed at 0 K. Future studies will be directed to using *ab initio* thermodynamics approaches,[28–30] to treat real SOFC operating conditions (temperature and partial oxygen pressure).

3. Results

3.1 Thermodynamic driving force for SSS

We first examined the properties of bulk $La_{0.5}Sr_{0.5}FeO_{3-\delta}$ (LSF) as a benchmark. The LSF displays a tetragonal structure (a = 5.462 Å; c = 7.743 Å) with the A-site cations forming a layered structure consisting of alternating LaO and SrO planes. It is known that the A-site cations take a random distribution at high temperature,[31] but our DFT calculations at zero temperature are done using the ordered layered structure which is found to be more stable than the homogenous distribution without entropic contribution and our unit cell size is too small to truly represent a random configuration. The ordered structure at low temperature is consistent with a previous study[32] suggesting that there is a significant size mismatch between A-site cations and the experimental observation of La-rich and Sr-rich cluster formation in Sr-doped $LaMnO_3$.[33] For the ideal LSF system, ferromagnetic and G-type antiferromagnetic are found to have similar energy (ferromagnetic phase is ~0.005 eV per cell lower). Huang *et al.* reported that $La_{0.58}Sr_{0.4}Co_{0.2}Fe_{0.8}O_{3-\delta}$ displays a ferromagnetic state below 200 K,[34] but the magnetic state may still change with temperature, ion deficiency, concentration of Co, strain, distribution of A-site cations and at the surface. For simplicity, we opt to use the ferromagnetic state for all calculations. When only one oxygen vacancy ($V_O^{\bullet\bullet}$, denoted using Kröger–Vink notation) is introduced, it prefers to occupy the LaO layer due to the largest $V_O^{\bullet\bullet}$ – B bond length which is opposite to the $V_O^{\bullet\bullet} - Sr'_{La}$ (Sr substitution of La) coupling as generally supposed. Also there is a preference for the $V_O^{\bullet\bullet}$ to locate closer to Co than Fe, because Fe (+1.88) prefers to be in a higher charge state than Co (+1.43), and the bond length of Co – $V_O^{\bullet\bullet}$ (1.918 Å) is smaller than Fe – $V_O^{\bullet\bullet}$ (1.958 Å) so that Co more easily accepts the extra charge left by $V_O^{\bullet\bullet}$ (which will be shown clearly below in Fig. 3). This is in agreement with experiment[35] and previous theoretical studies.[36] When more $V_O^{\bullet\bullet}$ are introduced, the preference for the single $V_O^{\bullet\bullet}$ to occupy the LaO layer is mitigated, pairs of $V_O^{\bullet\bullet}$ are found to prefer to occupy the opposite corner of the oxygen octahedron of a B cation. The $V_O^{\bullet\bullet}$ concentration in our calculation ranges from 1.43×10^{21} cm^{-3} to 2.86×10^{21} cm^{-3}.

Based on the above basic bulk properties and atomic configurations of LSCF, surface energy calculations of the low-index {001} (AO-BO_2), {110} (O_2-ABO), and {111} (B-AO_3) showed that the (001) orientation is most stable, which is chosen for the SSS calculations and analysis. In a (001) slab, one surface is terminated by the BO_2 plane, and the other surface by the AO plane, as shown in Fig. 1(a). The AO plane may consist of either LaO or SrO. To study SSS, for simplicity, we choose the LaO-terminated surface and then exchange the LaO atomic plane with one of the bulk SrO atomic planes in the middle of the slab as indicated in Fig. 1(a). More generally, partial exchange may occur which was not considered here. We then quantify the thermodynamic tendency of SSS by calculating the SSS energy as

$$E(\text{seg}) = [E(\text{SrO}) - E(\text{LaO})]/2A, \quad (3)$$

where E(seg) is the SSS energy, E(LaO) is the system energy for the LaO-terminated surface, and E(SrO) is the system energy for the SrO-terminated surface with the SrO surface formed by exchanging the original LaO surface layer with one bulk SrO layer centered in the middle of slab. Clearly, a smaller E(seg) indicates a larger SSS. Note that there are two different surfaces in the slab but the BO_2 surface remains the same before and after SSS, so to a good approximation, we can assume the surface energy and surface stress (see below) difference comes mainly from the AO surface only.

We identify two basic thermodynamic driving forces for SSS, surface stress/strain relaxation and surface charge minimization. First, the surface stress of the SrO-terminated surface is found to be smaller than that of the LaO-terminated surface (54 meV Å^{-2} *vs.* 136 meV Å^{-2} or 0.864 J m^{-2} *vs.* 2.176 J m^{-2}), indicating better strain relaxation in the SrO-terminated surface. The better strain relaxation in the SrO-terminated surface can be associated with the fact that the $La_{1-x}Sr_xFeO_3$ lattice constant decreases with increasing Sr concentration[35] so that the SrO surface layer relaxes strain more effectively under surface layer contraction conditions. On the other hand, the surface charge of the SrO-terminated surface (+0.52e) is found notably smaller than that of the LaO-terminated surface (+1.35e). Thus, the combined effects of smaller surface stress and smaller surface charge make the SrO-terminated surface to have lower surface energy than the LaO-terminated surface by 18 meV Å^{-2} (0.288 J m^{-2}), driving Sr to segregate to the surface. We note that usually the absolute surface energy of the solid surface falls in the range of ~100–500 meV Å^{-2} (1.6–8 J m^{-2}). DFT calculations are able to predict the relative stability of different surface reconstructions with a small surface energy difference down to ~1 meV Å^{-2} (0.016 J m^{-2}), such as the Si(001) surface reconstructions.[37]

3.1.1 Effect of strain on SSS in LSCF.

To further reveal and understand the effect of strain on SSS, we have calculated the dependence of SSS energy on strain by applying biaxial strain in the surface plane, and results for LSF and LSCF slabs are shown in Fig. 1(b). Similar to surface diffusion stress[38,39] and adsorption stress[40] that underlies the effect of strain on surface diffusion

and adsorption, we define a surface segregation stress as the surface stress difference before and after the SSS:

$$\Delta\sigma = \sigma(\mathrm{SrO}) - \sigma(\mathrm{LaO}), \quad (4)$$

where σ(SrO) and σ(LaO) are the surface stress of the SrO- and LaO-terminated surface after and before the SSS, respectively. Following linear elasticity theory, the effect of strain on the SSS energy can be calculated as

$$E_{\mathrm{seg}}^{\varepsilon} = E_{\mathrm{seg}}^{\varepsilon=0} + (\Delta\sigma_{xx} + \Delta\sigma_{yy})\varepsilon, \quad (5)$$

where $E_{\mathrm{seg}}^{\varepsilon}$ is the SSS energy under strain (ε) and $E_{\mathrm{seg}}^{\varepsilon=0}$ is the SSS without strain. So, to the first order, the SSS depends on strain linearly with a slope of surface segregation stress $\Delta\sigma$. The larger the $\Delta\sigma$ is, the stronger the strain dependence will be, and a given strain might either increase or decrease the SSS depending on the sign of $\Delta\sigma$. For LSF, our DFT+U calculations showed a small $\Delta\sigma \sim -42$ meV Å^{-2} (-0.672 J m^{-2}) indicating the SSS in LSF is weakly dependent on strain, which is indeed confirmed by our DFT+U calculations on applying strain, as shown in Fig. 1(b). For LSCF, $\Delta\sigma \sim -240$ meV Å^{-2} (-3.84 J m^{-2}) indicates a compressive surface segregation stress, namely the SSS tends to expand the surface, so that the SSS energy will decrease (increase) when a tensile (compressive) external strain is applied. This is again confirmed by DFT+U calculations as shown in Fig. 1(b). Therefore, a compressive strain will suppress the SSS in LSCF. This is consistent with the observation that the lattice constant of LSCF decreases nearly linearly with increasing Sr content[35] even though ionic radius of Sr is larger than that of La. Since strain always relaxes more effectively at a surface than in bulk, Sr prefers to stay in bulk under compressive strain and going to the surface under tensile strain. Moreover, this should be generally applicable as long as the lattice constant decreases with the increase in Sr concentration in any $La_{1-x}Sr_xBO_3$ system, for example, Jalili *et al.*[41] reported the similar strain-dependent behavior of Sr segregation in $La_{1-x}Sr_xMnO_3$.

3.1.2 Effect of surface charge on SSS in LSCF. To reveal the effect of surface charge on SSS, we introduce dopants into the cation site in LSCF and calculate the corresponding change in the SSS energy. The dopant concentration in our calculation is 1.43×10^{21} cm^{-3}. The dopant can be introduced to replace either B-site or A-site cations. For the B-site doping, the dopants with a higher charge state than the replaced B-site cations (such as Zr and Y) favor the surface positions to minimize surface charge, while the dopants with a lower charge state than the replaced B-site cations (such as Li) favor the bulk positions again to minimize surface charge. For the A-site doping, the dopants are found to prefer the surface AO planes mainly because the dopants we considered have a much smaller ionic radius than the A-site cation ionic radius, so that the strain effect dominates giving their preferred surface position even though their charge states might favor the bulk position.

So, generally speaking, because of ionic size and charge state difference between the dopant and host atom, doping may affect the SSS due to both strain and charge effects. By introducing the dopant with different charge states into the B-site, we found that the SSS is suppressed as a monotonic function of the absolute value of the BO_2 surface charge: the lower the absolute charge, the higher the SSS energy, as shown in Fig. 1(c). For the dopants with the same charge but different radii, it follows the expected strain dependence: the compressive strain suppresses the SSS, as shown in Fig. 1(c) for Al *vs.* Y and Ti *vs.* Zr. Doping of either Co or Fe B-site shows similar behavior, except the subtle difference of slightly smaller positive charge of Co than Fe.

For doping of the A-site with dopants of different charge state, the SSS energy is found to decrease monotonically with decreasing effective dopant charge state when the dopant are introduced into SrO layers, but increase monotonically with decreasing effective dopant charge state when the dopant are introduced into LaO layers, as shown in Fig. 1(d). This can be understood from the competition of occupying the surface AO layer by La *versus* Sr. By reducing the LaO surface charge through doping of a lower valence element in the La-site or conversely increasing the SrO surface charge through doping of higher valence elements in the Sr-site, the difference between SrO and LaO surface charge is reduced, and hence the SSS is suppressed.

3.2 Ways for suppressing SSS

Based on the basic driving forces we identified above, we suggest two possible ways to suppress SSS in LSCF: introduce compressive strain and reduce surface charge, which can be realized by following methods listed in Table 1. First, compressive strain can be applied either *via* introduction of larger dopants, or interface lattice mismatch between LSCF and certain electrolytes, or adding some surface coating layer that can provide compressive strain on LSCF. Second, the dopant can be introduced into the cation site to alter the surface charge as needed, specifically, decreasing LaO or BO_2 surface charge, or increasing SrO surface charge. In addition, Co substitution of Fe, $V_O^{\bullet\bullet}$ formation, and formation of A-site cation deficiency can be used to induce both strain and change of surface charge. While generally reducing the $V_O^{\bullet\bullet}$ and Co content suppresses SSS which is beneficial for SOFC cathode durability, on the other hand, it is worth noting that an optimized $V_O^{\bullet\bullet}$ and Co content needs to be determined to reach a delicate balance between keeping the appreciable suppression of

Table 1 Common factors for suppressing SSS

(1) Apply compressive strain	Introduce larger dopant	Reduce Co concentration
	Apply epitaxial strain/coating	Reduce $V_O^{\bullet\bullet}$ concentration
(2) Reduce surface charge	Decrease BO_2 surface charge	Create A-site deficiency
	Decrease LaO surface charge	
	Increase SrO surface charge	

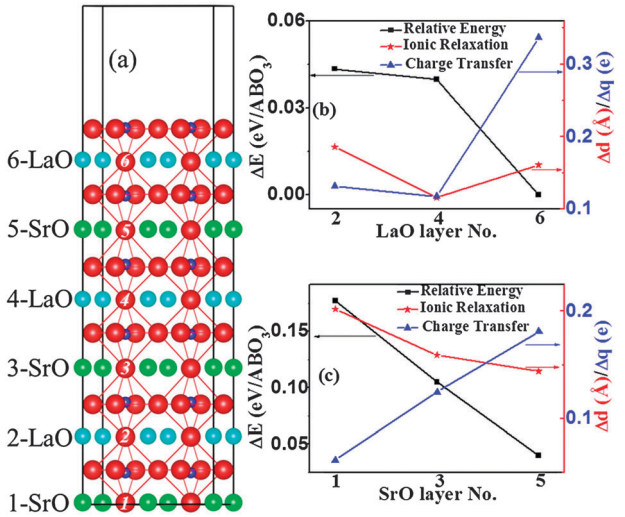

Fig. 2 (a) The location of $V_O^{\bullet\bullet}$ in the LSF slab. Cyan balls are La atoms, green are Sr, red are O, and small blue are Fe. (b) LaO layer properties: squares are relative energy of $V_O^{\bullet\bullet}$ located at different LaO layers as denoted in (a), with the "6-LaO" energy set as a reference of zero energy, triangles are the corresponding charge transfer, and stars are ionic relaxation. (c) SrO layer properties, the symbols are the same as in (b).

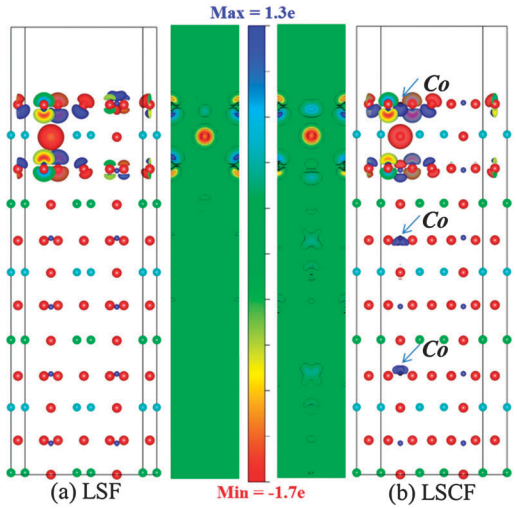

Fig. 3 Charge density difference plots upon $V_O^{\bullet\bullet}$ formation. (a) LSF slab. (b) LSCF slab. Blue (red) cloud represents accepted (donated) charge. Cyan atoms are La, green atoms are Sr, red atoms are O, and small blue atoms are Fe; Co atoms are marked by arrows.

SSS and maintaining the good mixed ionic and electronic conductivity of LSCF.

3.3 More on SSS and suppression of SSS in LSCF

3.3.1 Effect of $V_O^{\bullet\bullet}$ on SSS in LSCF. We first determine the preferred $V_O^{\bullet\bullet}$ location by calculating the relative energy for $V_O^{\bullet\bullet}$ occupying different AO layers, as denoted in Fig. 2(a). Fig. 2(b) and (c) show the calculated energies for LaO and SrO layers, respectively. In general, we found that $V_O^{\bullet\bullet}$ favors the LaO layers over the SrO layers and the most stable location is the subsurface layer [denoted as "6-LaO" in Fig. 2(a)], which is set as the reference of zero energy. Also plotted are charge transfer and ionic relaxation, derived from the neighboring B-site cations of $V_O^{\bullet\bullet}$, due to $V_O^{\bullet\bullet}$ creation at different layers. It is somewhat surprising that ionic relaxation contribution to determining the $V_O^{\bullet\bullet}$ position is negligible, which is opposite to what people normally think, like in YSZ.[42] A possible reason is that LSCF is a good electron conductor in which charge transfer is a more dominant effect than strain to affect energy. We found that there is close correlation between the $V_O^{\bullet\bullet}$ formation energy and charge transfer: the larger the charge transfer is, the lower the energy will be; the lowest energy configuration of $V_O^{\bullet\bullet}$ in the subsurface 6-LaO layer shows the largest charge transfer. The reason for the largest charge transfer occurs in the subsurface layer is that the distance between $V_O^{\bullet\bullet}$ and neighboring surface B-cation is decreased relative to the bulk so that neighboring surface B-cations accept more charge while the cation octahedron surrounding $V_O^{\bullet\bullet}$ remains intact, and this applies to all possible AO layer terminations. The same preferred $V_O^{\bullet\bullet}$ location is found in LSCF, although the charge transfer upon $V_O^{\bullet\bullet}$ creation appears relatively localized among the $V_O^{\bullet\bullet}$-containing AO layer and its neighboring layers in LSF as shown by the charge difference plot in Fig. 3(a), while the charge transfer spreads over the whole slab in LSCF, with all the Co atoms accepting extra charge from the electrons left by $V_O^{\bullet\bullet}$ formation independent of the $V_O^{\bullet\bullet}$ – Co distance, as shown by the charge difference plot in Fig. 3(b).

Using the preferred $V_O^{\bullet\bullet}$ location, we calculated the SSS in LSCF and found that $V_O^{\bullet\bullet}$ enhances slightly the SSS lowering the SSS energy by $\sim$1 meV Å^{-2} (0.016 J m^{-2}). This qualitatively agrees with the experimental finding by Fister *et al.*[43] that the SSS becomes larger with decreasing oxygen pressure, since lower oxygen pressure should result in more $V_O^{\bullet\bullet}$ in LSCF. To understand this enhancement, it is natural to notice that $V_O^{\bullet\bullet}$ introduction induces the following two changes. First, in terms of surface charge, the BO_2 surface becomes more negatively charged since it accepts the extra charge left by $V_O^{\bullet\bullet}$ for being the neighboring layer of $V_O^{\bullet\bullet}$, which drives the more positively charged LaO layer next to the BO_2 surface, leaving Sr behind to form the Sr-rich surface. The preferred $V_O^{\bullet\bullet}$ occupation in the subsurface LaO layer makes the subsurface be mostly composed of La, leaving the surface AO layer to be more occupied by Sr as the A-site cations form alternating parallel planes. Second, in terms of strain, although the creation of $V_O^{\bullet\bullet}$ causes compressive strain, consistent with previous findings,[3] which would suppress SSS, the increased surface charge effect and the preferred subsurface location of $V_O^{\bullet\bullet}$ make $V_O^{\bullet\bullet}$ overall an enhancer for SSS.

3.3.2 Effect of Co on SSS in LSCF. When Co atoms are introduced to replace a quarter of Fe atoms in the slab, they prefer to stay in the bulk if without $V_O^{\bullet\bullet}$ but in the surface if $V_O^{\bullet\bullet}$ is present for the reason that $V_O^{\bullet\bullet}$ prefers to form in the LaO subsurface layer and to be the nearest neighbor of Co, so that more charge transfer can occur due to the shorter $V_O^{\bullet\bullet}$ – Co distance under surface contraction if Co atoms occupy surface sites. Similar to $V_O^{\bullet\bullet}$, Co is found to enhance the SSS lowering the SSS energy by $\sim$5 meV Å^{-2} (0.08 J m^{-2}) due to two reasons. First, in terms of strain, because the lattice constant of LSCF

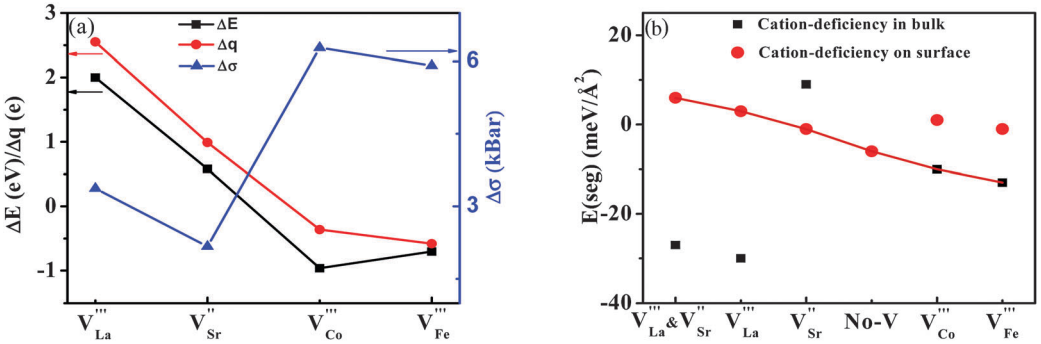

Fig. 4 (a) Cation-deficiency occupation position preference. Δq denotes difference of surface charge between vacancy occupying surface and bulk defined as q(bulk) − q(surface), $\Delta\sigma$ denotes the decrease of system stress defined as σ(bulk) − σ(surface), and ΔE denotes change of system energy defined as E(bulk) − E(surface). (b) Effect of deficiency on SSS in LSCF; data on the line denote the preferred occupation sites.

decreases with increasing Co content,[44] Co doping induces tensile strain, which tends to enhance SSS. Second, in terms of surface charge, the BO_2 surface becomes more negatively charged because the effective charge of Co is smaller than that of Fe, attracting La to the subsurface of the BO_2 terminated surface and leaving behind more Sr to occupy the AO-terminated surface at the same time, enhancing the SSS.

In addition, we found that although both $V_O^{\bullet\bullet}$ and Co enhance the SSS separately, their combined effect lowering the SSS by ~3 meV Å^{-2} (0.048 J m^{-2}) is smaller than the effect of Co alone. One possible reason for this is that $V_O^{\bullet\bullet}$ and Co introduce opposite strain effects, the former compressive while the latter tensile, which compensate each other hereby reducing the overall strain effect.

3.3.3 Introduction of cation deficiency. In experiment, cation deficiency is always used in trying to improve the performance of SOFCs, and Hansen[45] reported that A-site deficient LSCF suppresses the SSS. Here the cation deficiency effect on SSS is studied for every cation species at the concentration of 1.43 × 10^{21} cm^{-3}, which is within the experimental accessible values.[45] It is found that the A-site cation deficiency prefers to occur at the surface while the B-site cation deficiency occurs in bulk mainly because of the surface charge minimization effect. As the stoichiometric AO surface is positively charged while the BO_2 surface is negatively charged, cation vacancy in the AO surface is favored as it decreases surface charge while cation vacancy in the BO_2 surface is forbidden because it increases surface charge. Fig. 4(a) shows the energy difference, ΔE = E(bulk) − E(surface), where E(bulk) and E(surface) denote the system energy for cation deficiency with the cation removed from bulk and surface positions, respectively, along with the corresponding change of charge (Δq, red dots) and stress ($\Delta\sigma$, blue triangles). From the energy curve, we can see that the A-site deficiency favors surface positions (positive energy), while the B-site deficiency favors bulk positions (negative energy). We also see that the preferred cation deficiency position is mainly determined by the surface charge minimization effect, as there is a close correlation between ΔE and Δq, but not so for $\Delta\sigma$, indicating the stress effect is less important here.

Fig. 4(b) shows the calculated SSS energy for different cation-deficiency configurations using the preferred A-site surface deficiency and B-site bulk deficiency positions as determined above (line connected data points, also both vacancy occupation in bulk (black squares) and on the surface (red circles) are provided for reference). We see that the A-site surface deficiency suppresses the SSS (positive segregation energy), while the B-site bulk deficiency enhances the SSS (negative energy). The A-site suppression can be understood in terms of a surface charge decrease, and the B-site enhancement in terms of introducing bulk tensile strain.

3.3.4 LSM-coating on LSCF. As recently reported by Lynch *et al.*,[17] the LSM coating suppresses SSS in LSCF. It was found that Co goes to LSM, forming a hybrid $La_{1-x}Sr_xCo_{1-y}Mn_yO_{3-\delta}$ (LSCM) phase, and also $V_O^{\bullet\bullet}$ concentration is increased in LSM. To better understand their experiments, we have performed first principles calculations to study the effect LSM coating on the SSS in LSCF and in particular to see whether the above-mentioned two factors can be applied in this case. Fig. 5(a) shows the preferred $V_O^{\bullet\bullet}$ location between LSCF and LSM layers. Without Co, $V_O^{\bullet\bullet}$ favors LSM (first data point); with Co only in LSCF but not LSM, $V_O^{\bullet\bullet}$ favors LSCF (second data point); with Co in both LSCF and LSCM, $V_O^{\bullet\bullet}$ favors LSCM (last three data points). This suggests that $V_O^{\bullet\bullet}$ prefers to occupy next to Co, indicating a strong Co − $V_O^{\bullet\bullet}$ binding, which is further shown by the increasing binding energy with the increasing Co concentration (last two data points). Fig. 5(b) shows the energy difference between Co in LSM/LSCM and in LSF/LSCF, using the latter as the reference of zero energy. Since $V_O^{\bullet\bullet}$ prefers to be in LSM, as found in Fig. 5(a), we can conclude that Co prefers occupying LSM/LSCM from Fig. 5(b) (last two triangle data points). Fig. 5(c) shows the SSS energy in LSM coated LSCF for different $V_O^{\bullet\bullet}$ and Co configurations. We see that $V_O^{\bullet\bullet}$ and/or Co occupying LSM layers suppresses SSS. The more Co atoms locating at LSM, the stronger suppression of SSS in LSCF will be, regardless of the presence and location of $V_O^{\bullet\bullet}$ (last three data points). Fig. 5(d) shows the overall LSM coating effect on the SSS energy in LSCF, calculated from the optimized $V_O^{\bullet\bullet}$ and Co configurations. It clearly indicates that LSM-coating always strongly suppresses SSS in LSCF. The suppression is caused by the occupation of $V_O^{\bullet\bullet}$ in LSM, the occupation of Co in LSM, and compressive strain under LSM coating (LSM 3.87 Å[46] *vs.* LSCF

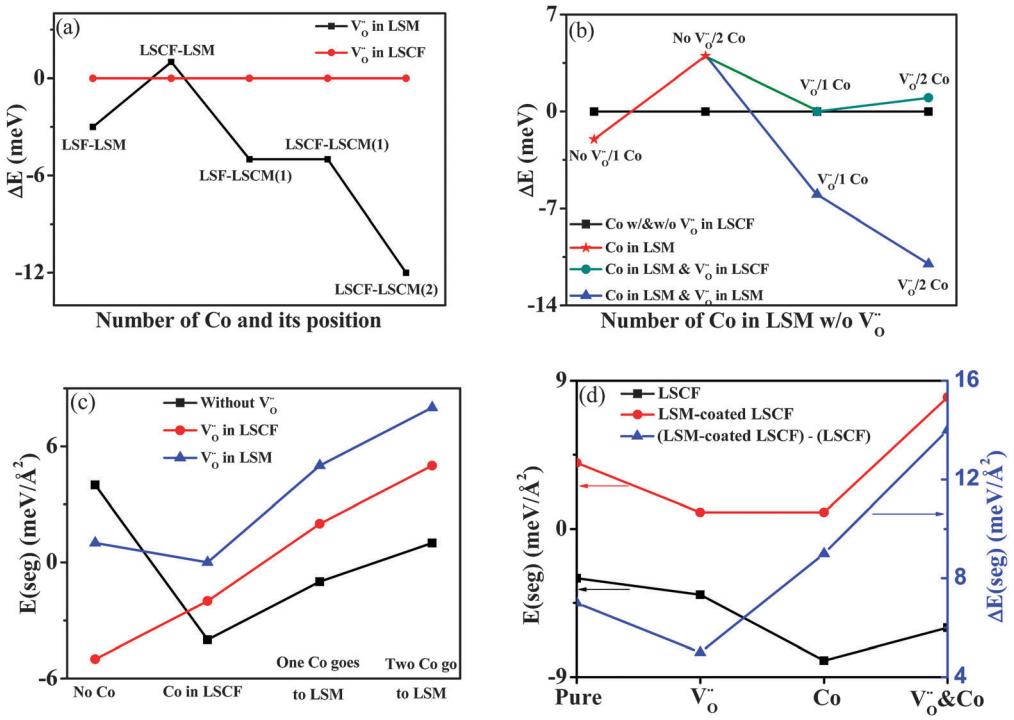

Fig. 5 (a) The location of $V_O^{\bullet\bullet}$ in LSM-coated LSCF, $V_O^{\bullet\bullet}$ occupying LSCF is set as reference. *X* in ''LSCM(*X*)'' denotes the number of Co atoms in LSM. (b) The location of Co in LSM-coated LSCF, Co with/without $V_O^{\bullet\bullet}$ occupying LSCF (and $V_O^{\bullet\bullet}$ occupying LSCF if applicable) is set as reference. *X* in ''*X* Co'' denotes the number of Co atoms in LSM. (c) Effect of $V_O^{\bullet\bullet}$ and Co location on SSS in LSM-coated LSCF. (d) Comparison of SSS between LSCF and LSM-coated LSCF, right *y*-axis and triangle data denote the *E*(seg) differences between LSCF and LSM-coated LSCF. $V_O^{\bullet\bullet}$ (Co) denotes that only the oxygen vacancy (Co atom) was introduced into the system, and $V_O^{\bullet\bullet}$ and Co denotes that both are introduced into the system simultaneously.

3.93 Å[47]). Furthermore, because we exchanged the position of Co and Mn in the calculation for Co occupying LSM, the presence of Mn in LSCF introduces compressive strain, which helps the suppression too. It is also interesting to point out that the magnitude of enhancement surprisingly decreases for the case with only $V_O^{\bullet\bullet}$ introduced into the system even though $V_O^{\bullet\bullet}$ occupying LSM tends to further suppress SSS (first two data points). This is because an increased lattice constant of LSM and decreased lattice constant of LSF when $V_O^{\bullet\bullet}$ is changed from LSF into LSM, which leads to decreased compressive strain applied on LSF by LSM, thus hinders the suppression of SSS. These are consistent with experimental observations.[17]

On the other hand, it is also reported that by using PSM as a coating layer,[48] the performance enhancement is more significant. A possible reason is that, compared to LSM, the preference of $V_O^{\bullet\bullet}$ occupation in the PrO layer is even stronger compared to the LaO layer, which is 0.20 eV lower according to our calculation, promoting more $V_O^{\bullet\bullet}$ from LSCF into the PSM coating layer, and hence inducing larger suppression of SSS in LSCF.

4. Conclusions

We have performed a systematic first principles study on SSS in LSCF. We found two basic thermodynamic driving forces for SSS: surface charge minimization and strain relaxation. Based on this finding, we suggest two possible ways to suppress SSS: applying compressive strain and reducing surface charge. We then illustrated several possibilities of affecting these two factors individually or together, through oxygen vacancy, Co substitution of Fe, and cation site deficiency. Finally, we applied our theoretical findings to explain recent experimental observations of suppression of SSS in LSCF by LSM and PSM coating in terms of these two factors. We believe that some of our findings on SSS and suppression of SSS are generally applicable in common perovskite $La_{1-x}Sr_xBO_3$ materials.[49,50]

Acknowledgements

We thank Emily A. Carter for helpful discussions. We acknowledge the financial support from DOE EFRC Grant Number DE-SC0001061 as a flow through from the University of South Carolina. We also thank DOE-NERSC, Fusion at LCRC at Argonne National Laboratory, and CHPC at the University of Utah for providing computing resources.

References

1 L. Yang, S. Z. Wang, K. Blinn, M. F. Liu, Z. Liu, Z. Cheng and M. L. Liu, *Science*, 2009, **326**, 126.
2 http://www.netl.doe.gov/publications/proceedings/11/seca/pdf/Tue%20AM/Vora.2011_07_26_SECA.pdf.
3 S. Wang, M. Katsuki, M. Dokiya and T. Hashimoto, *Solid State Ionics*, 2002, **152–153**, 777.

4 M. Becker, A. Mai, E. Iver-Tiffee and F. Tietz, *Solid Oxide Fuel Cells, The Electrochemical Society Proceedings Series*, Pennington, NJ, 2005, p. 514.
5 A. Mai, M. Becker, W. Assenmacher, F. Tietz, D. Hathiramani, E. Ivers-Tiffee, D. Stover and W. Mader, *Solid State Ionics*, 2006, **177**, 1965.
6 D. Oh, E. Armstrong, D. Jung, C. Kan and E. Wathsman, *ECS Trans.*, 2009, **25**, 2871.
7 P. Tanasini, M. CAnnarozzo, P. Costamagna, A. Faes, J. Van Herle, A. Hessler-Wyser and C. Comninellis, *Fuel Cells*, 2009, **9**, 740.
8 C. Haering, A. Roosen and H. Schichl, *Solid State Ionics*, 2005, **176**, 253.
9 S. Li, W. Jin, P. Huang, N. Xu, J. Shi and Y. S. Lin, *J. Membr. Sci.*, 2000, **166**, 51.
10 Z. Shao and S. M. Haile, *Nature*, 2004, **431**, 170.
11 W. Jung and H. L. Tuller, *Energy Environ. Sci.*, 2012, **5**, 5370.
12 E. J. Crumlin, E. Mutoro, Z. Liu, M. E. Grass, M. D. Biegalski, Y. L. Lee, D. Morgan, H. M. Christen, H. Bluhm and Y. Shao-Horn, *Energy Environ. Sci.*, 2012, **5**, 6081.
13 P. A. W. V. Heide, *Surf. Interface Anal.*, 2002, **33**, 414.
14 J. E. Elshof, H. J. M. Bouwmeester and H. Verweij, *Appl. Catal., A*, 1995, **130**, 195.
15 H. Dullli, P. A. Dowben, S. H. Liou and E. W. Plummer, *Phys. Rev. B: Condens. Matter Mater. Phys.*, 2000, **62**, R14629.
16 W. A. Harrison, *Phys. Rev. B: Condens. Matter Mater. Phys.*, 2011, **83**, 155437.
17 M. E. Lynch, L. Yang, W. Qin, J. Choi, M. Liu, K. Blinn and M. Liu, *Energy Environ. Sci.*, 2011, **4**, 2249.
18 F. Liu, F. Wu and M. G. Lagally, *Chem. Rev.*, 1997, **97**, 1045.
19 H. Hu, H. J. Gao and F. Liu, *Phys. Rev. Lett.*, 2008, **101**, 216102.
20 M. J. Asaro and W. A. Tiller, *Metall. Trans.*, 1972, **3**, 1789.
21 X. B. Niu, G. B. Stringfellow and F. Liu, *Phys. Rev. Lett.*, 2011, **107**, 076101.
22 W. Siemons, G. Koster, H. Yamamoto, W. A. Harrison, G. Lucovsky, T. H. Geballe, D. H. A. Blank and M. R. Beasley, *Phys. Rev. Lett.*, 2007, **98**, 196802.
23 G. Kresse and J. Hafner, *Phys. Rev. B: Condens. Matter Mater. Phys.*, 1996, **54**, 11169.
24 L. Wang, T. Maxisch and G. Ceder, *Phys. Rev. B: Condens. Matter Mater. Phys.*, 2006, **73**, 195107.
25 W. Tang, E. Sanville and G. Henkelman, *J. Phys.: Condens. Matter*, 2009, **21**, 084204.
26 V. Dusastre and J. A. Kilner, *Solid State Ionics*, 1999, **126**, 163.
27 I. Barin, *Thermochemical Data of Pure Substances*, 3rd edn, 2008.
28 C. Lee, R. Behera, E. Wachsman, S. Phillpot and S. Sinnott, *Phys. Rev. B: Condens. Matter Mater. Phys.*, 2011, **83**, 115418.
29 Y. Mastrikov, R. Merkle, E. Heifets, E. Kotomin and J. Maier, *J. Phys. Chem. C*, 2010, **114**, 3017.
30 Y. Mastrikov, E. Heifets, E. Kotomin and J. Maier, *Surf. Sci.*, 2009, **603**, 326.
31 Z. L. Wang and J. Zhang, *Phys. Rev. B: Condens. Matter Mater. Phys.*, 1996, **54**, 1153.
32 A. Chroneos, B. Yildiz, A. Tarancon, D. Parfitt and J. A. Kilner, *Energy Environ. Sci.*, 2011, **4**, 2774.
33 T. Shibata, B. Bunker, J. F. Mitchell and P. Schiffer, *Phys. Rev. Lett.*, 2002, **88**, 207205.
34 B. Huang, J. Malzbender and R. W. Steinbrech, *J. Mater. Res.*, 2011, **26**, 1388.
35 L.-W. Tai, M. M. Nasrallah, H. U. Anderson, D. M. Sparlin and S. R. Sehlin, *Solid State Ionics*, 1995, **76**, 259–273.
36 M. Pavone, A. M. Ritzmann and E. Carter, *Energy Environ. Sci.*, 2011, **4**, 4933.
37 F. Liu and M. G. Lagally, *Phys. Rev. Lett.*, 1996, **76**, 3156.
38 D. J. Shu, F. Liu and X. G. Gong, *Phys. Rev. B: Condens. Matter Mater. Phys.*, 2001, **64**, 245410.
39 L. Huang, F. Liu, G. H. Lu and X. G. Gong, *Phys. Rev. Lett.*, 2006, **96**, 016103.
40 R. Pala and F. Liu, *J. Chem. Phys.*, 2004, **120**, 7720.
41 H. Jalili, J. W. Han, Y. Kuru, Z. Cai and B. Yildiz, *J. Phys. Chem. Lett.*, 2011, **2**, 801.
42 H. Ding, A. V. Virkar and F. Liu, *Solid State Ionics*, 2012, **215**, 16.
43 T. Fister, D. Fong, J. Eastman, P. Baldo, M. Highland, P. Fuoss, K. Balasubramaniam, J. Meador and P. Salvador, *Appl. Phys. Lett.*, 2008, **93**, 151904.
44 J. N. Kuhn and U. S. Ozkan, *Catal. Lett.*, 2008, **121**, 179.
45 K. K. Hansen and K. V. Hansen, *Solid State Ionics*, 2007, **178**, 1379.
46 S. Dussan, A. Kuman and R. S. Katiyar, *MRS Online Proc. Libr.*, 20091199-F03-05.
47 J. S. Hardy, J. W. Templeton, D. J. Edwards, Z. Lu and J. W. Stevenson, *J. Power Sources*, 2012, **198**, 76.
48 http://www.netl.doe.gov/publications/proceedings/11/seca/pdf/Poster%20Presentations/Ding.pdf.
49 S. Piskunov, E. Heifets, T. Jacob, E. Kotomin, D. Ellis and E. Spohr, *Phys. Rev. B: Condens. Matter Mater. Phys.*, 2008, **78**, 121406.
50 E. Heifets, E. Kotomin, Y. Mastrikov, S. Piskunov and J. Maier, *Thermodynamics – Interaction Studies – Solids, liquids and gases*, InTech Open Access Publishers, 2011, p. 491.

